15TH IEA HEAT PUMP CONFERENCE
MAY 26–29, 2026 | HOFBURG
VIENNA 2026
DECARBONISATION THROUGH INNOVATION

A Machine Learning (ML) model for performance prediction control strategy for a dual-source direct-expansion solar-assisted transcritical carbon-dioxide heat pump

F. Di Salvatore[a], A. W. Mauro[a*], M. Pieve[b], V. Piscopo[a], R. Trinchieri[b], D. Urbano[b], L. Viscito[a]

[a]Department of Industrial Engineering, Università degli Studi di Napoli–Federico II, P.le Tecchio 80, 80125 Naples, Italy
[b]ENEA National Agency – Casaccia Research Centre, Via Anguillarese, 301, Roma 00123, Italy

Abstract

In accordance with the progressive electrification of energy consumption outlined by European Community policies and given the expected increase in the use of heat pumps to replace traditional heating systems based on fossil fuels combustion, it is essential to predict the performance of these machines and develop reliable control strategies to ensure their efficient and sustainable operation. To address this challenge, this work develops a data-driven methodology for real-time source selection in a direct-expansion dual-source heat pump prototype working with carbon-dioxide as working fluid, by combining experimental measurements with Machine Learning-based performance modelling. The system, with a heating capacity of about 15 kW and equipped with both finned-coil heat exchanger and hybrid photovoltaic-thermal panels as evaporators, was tested for domestic hot water application with a temperature lift from 20°C to 60°C in a range of compressor frequencies between 50÷60 Hz, ambient temperature of 16÷25°C and solar irradiances of approximately 225÷725 W/m^2. Based on this data, Artificial Neural Networks were then trained to predict the prototype performances only considering boundary conditions such as ambient temperature and solar irradiance to generate dense performance maps across the operating domain. Thanks to these performance maps, it was possible to reconstruct, for each compressor frequency, an irradiance threshold curve as a function of ambient temperature, above which the Sun-Mode heat pump operation outperforms the Air-Mode operation. This approach provides a basis for reliable, real-time supervisory control strategies for dual-source solar-assisted CO_2 heat pumps.

Selection and/or peer-review under the responsibility of the organizers of the 15th IEA Heat Pump Conference 2026.

Keywords: Solar-assisted; Predictive control; Machine Learning; Dual-source; Carbon-dioxide

1. Introduction

The household sector is responsible for approximately 26% of Europe's final total energy consumption, with nearly 78% of this used for space heating and domestic hot water (DHW), and more than half still supplied by fossil-fuel-based systems [1] [2]. Achieving the carbon-neutrality targets of the European Green Deal [3] by 2050 requires both a substantial increase of renewable electricity production and the widespread adoption of sustainable heating technologies. Heat pumps have emerged as a commercially mature solution, capable of reducing CO_2 emissions by about 500 million tons by 2030 if widely deployed [4] [5].

However, their efficiency remains strongly dependent on the temperature of the available heat source, in fact conventional air-source heat pumps suffer significant performance drops at low ambient temperatures,

* Corresponding author. Tel.: +39 0817682198
E-mail address: wmauro@unina.it

precisely when heating demand is higher [6].

Multi-source architectures [7], and solar-assisted heat pumps [8] , have been proposed to overcome the performance limitations of conventional air-source units. Some of these systems can employ several "solar evaporators" such as hybrid photovoltaic-thermal (PV/T) modules that can be used in both direct (DX) and indirect (IDX) expansions configurations or conventional solar collectors (SC), mainly used in indirect expansion configurations. In DX dual-source heat pumps equipped with PV/T systems, the refrigerant evaporates directly in the tubes mounted on the back of the panels, whereas in indirect-expansion layouts a secondary fluid, such as water [9] or water-glycol mixture [10] transfers heat from the collector to the refrigerant. Both approaches can increase the effective evaporation temperature, improving system efficiency and, in the case of PV/T, also providing thermal management for the panels. However, the actual performance gains of these hybrid solutions depend strongly on solar irradiance, ambient temperature and on the control strategy that chose when and how to switch between sources.

Despite previous research regarding CO_2 use in air-to-water and multi-ejector applications [11] [12], few studies have explored CO_2 in dual-source DX configurations with integrated solar evaporators [13], and research on dynamic control strategies [14] that select the most efficient heat source based on ambient temperature and solar irradiance is poor. In this context, machine-learning models trained on experimental data can provide robust boundary-condition-based predictions of COP and heating capacity, supporting real-time source-switching decisions.

This study presents the experimental characterization of a DX solar-assisted CO_2 heat pump prototype, equipped with both air and PV/T evaporators and the development of AI-based models (Artificial Neural Networks, ANN) trained on prototype’s measured data to predict its COP and gas-cooler heating capacity. Also, thanks to the data generated from the model it is possible to identify an irradiance threshold above which Sun-Mode outperforms Air-Mode.

The paper is organized as follows. Section 2 describes the heat pump prototype and the measurement setup. Section 3 outlines the experimental methodology and the operating condition while section 4 presents the development of the ANN models with the calibration and validation procedure. Section 5 discusses the performance comparison between Air-Mode and Sun-Mode and introduces the methodology used to identify the irradiance threshold. Finally, Section 6 summarizes the main findings and highlights future research directions.

2. System Description

2.1. Experimental setup and system layout

The investigated system is a direct-expansion dual-source solar-assisted heat pump (DX-SAHP) using CO2 as working fluid and is installed at ENEA Casaccia Research Centre (Rome, Italy). The experimental apparatus, with a maximum heating capacity of approximately 15 kW, combines a standard air-to-water heat pump with a photovoltaic (PV) field made up of two strings of five photovoltaic-thermal hybrid panels (PV/T), with a total installed area of about 14.5 m^2, that can also be used as an alternative to the finned coil heat exchanger for the heat pump evaporation process.

In fact, a portion of the solar radiation incident on PV panels is not converted into electrical energy but is absorbed by the panels, leading to their overheating. By integrating some coils on the back side of the panel, through which the refrigerant flows, this heat can be recovered to drive the refrigerant evaporation process. At the same time, the overheating of the panel is prevented, keeping it within an optimal operating temperature range [15] [16]. For this reason, the heat pump can operate in heating mode by using the finned-coil heat exchanger in “Air-mode” and the PV/T panels in “Sun-mode” as evaporators. A picture of the prototype is shown in Figure 1.

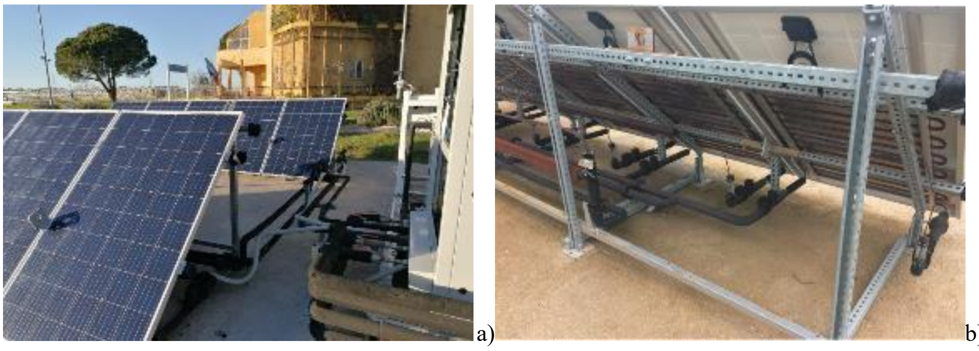
a) b)

Figure 1. Picture of the front side of the panels (a) and the refrigerant circuit mounted on the rear (b).

The prototype consists of an inverter-driven compressor (displacement of 10 cm^3/rev), which compresses the refrigerant to high-pressure and high-temperature conditions. After the compressor, a brazed-plate heat exchanger is installed and operates as a gas cooler (GC), enabling heat rejection to the secondary water loop and raising the water temperature to the desired level.

The refrigerant then flows through a second plate heat exchanger, which acts as an internal heat exchanger (IHX). At its outlet, an electronic expansion valve (EEV) reduces the pressure to the low-pressure side of the thermodynamic cycle.

Depending on the selected evaporation source, an appropriate valve arrangement directs the refrigerant either to a finned-coil heat exchanger (Air-Mode operation, Figure 2a) or to a sheet-and-tube heat exchanger mounted on the back of the photovoltaic panels (Sun-Mode operation, Figure 2b), where the evaporation process takes place.

The refrigerant leaving the evaporator has a high vapor quality (between 0.95 and 0.98) and subsequently enters a liquid receiver (LR), where it is drawn from the upper section and split into two streams by means of a bypass valve. While one is directed to the IHX, the other one flows directly toward the suction line, where the two streams recombine providing the certain degree of superheating and preventing liquid from reaching the compressor suction.

A secondary hydraulic loop manages the conditions of water entering and leaving the gas cooler to maintain stable working conditions. Specifically, a 300-liter water tank is cooled by an electric chiller and a dry cooler to stabilize the inlet temperature, while the outlet water temperature from the gas cooler is regulated by a PID controller which adjusts the water flow rate delivered by the circulation pump in proportion to the control signal, in order to meet the desired temperature setpoint.

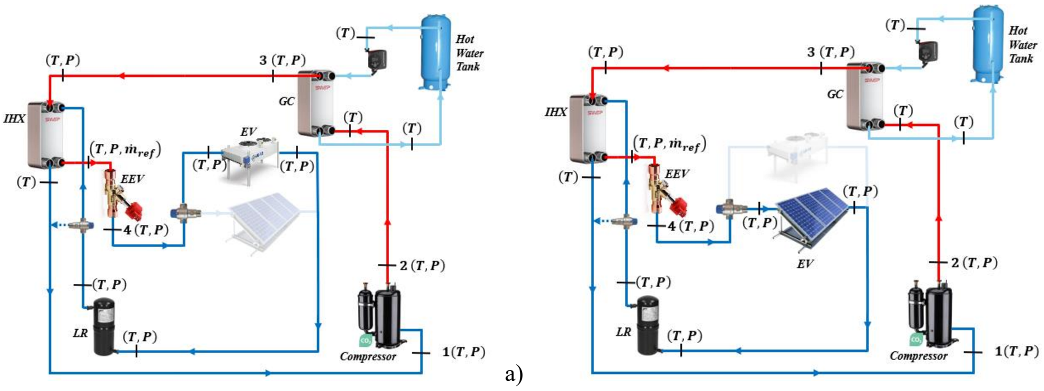

a) b)

Figure 2. Schematic of the experimental setup in air-mode a) and sun-mode b).

For monitoring the heat pump operation, several sensors have been installed. Specifically, T-type thermocouples measure the inlet and outlet temperatures of each component of the prototype; also, 10 absolute pressure transducers were installed at the inlet and outlet of the main refrigerant-loop components to monitor their pressure levels.

Finally, two wattmeters measure the electrical power absorbed by the heat pump and the total electrical power produced by the PV/T panels, while a Coriolis flowmeter and a pyranometer are used to measure, respectively, the refrigerant mass flow rate and the solar irradiance incident on the panels. Table 1 highlights the main features of the installed sensors. Relative uncertainties are expressed as a percentage of the measured values.

Table 1. Main features of the sensors installed on the prototype.

Sensor	Measured variable	Range	Uncertainty
T-type Thermocouples	Temperature [°C]	$-40 \div 350$	$\pm 0.2\,°C$
Coriolis Flowmeter	Mass flow [kg/s]	0.008 ÷ 0.25	± 0.1 %
Pressure Transducer	Pressure [bar]	up to 160	± 0.1 %
Pyranometer	Solar radiation [W/m^2]	0 ÷ 2000	± 1 %
Wattmeters	PVs total output power and heat pump total absorption [kW]	up to 40	± 0.1 %

2.2. PV/T evaporator

The solar evaporator is made of a sheet and tube heat exchanger: the tubes are bonded with a thermal adhesive paste to a thin aluminium sheet mounted on the rear of the panels. The PV panels in each string are electrically connected in series while the two strings are connected in parallel; they are made of polycrystalline silicon cells with a peak power of 270 W and are installed with a tilt angle of 48.2° relative to the horizontal.

Since the system is not equipped with a solar tracker, the angle of incidence (AOI) of the solar radiation on the collector plane varies throughout the day. During the experimental campaign solar-mode tests were conducted between 10:00 and 15:00 with typical values of AOI between 10° and 55°.

The tubes, with an outer diameter of 8 mm and made of copper, are fed in parallel by the refrigerant; each circuit comprises 10 tubes with a pitch of 80 mm. Table 2 summarises the electrical characteristics of the PV modules and the geometric features of the solar heat exchanger's tubes.

Table 2. PV modules and solar heat exchanger main features.

PV modules		Sheet and tube heat exchanger	
Dimensions	1650x992x40 mm	External tube diameter	8 mm
Cell Type	Polycrystalline silicon	Tube pitch	80mm
Cell Size	156x156 mm	Number of tubes	10
Number of cells	60	Tube material	Copper
Peak power	270 W		
Tilt Angle	48.2°		
Incidence Angle	10°÷55°		

3. Experimental campaign

3.1. Experimental procedure and text matrix

The experimental campaign was performed the 2025 spring season at the ENEA Casaccia Research Center (Rome, Italy 42.04° N, 12.30° E), with the aim of characterizing the performance of the prototype in both air-mode and sun-mode operation. The tests focused on DHW production under fixed sink temperature conditions, with a temperature lift from 20 °C at the gas cooler (GC) water inlet to 60 °C at the GC water outlet. These temperatures were maintained constant during each experiment by means of an external chiller, while varying the compressor frequency and operating under different ambient temperature and solar irradiance conditions. This approach enabled coverage of a wide range of operating conditions, as summarized in the test matrix reported in Table 3. All tests were conducted under real PV/T field operating conditions to ensure that the measured performance is representative of actual in-field operation.

Table 3. Test matrix.

	Air Mode		Sun Mode	
f_{comp} $[Hz]$	T_{amb} $[°C]$	$\dot{V}_{air}$ $[m^3/h]$	$T_{amb}[°C]$	G $[W/m^2]$
50	16.9 ÷24.8	4500	17.4÷24.9	275÷725
55	16.1÷24.1	4500	16.3÷24.5	226÷727
60	15.9÷24.7	4500	16.7÷24.6	264÷692

Sensor signals are acquired using data acquisition (DAQ) boards, converted into digital data, and displayed in the user interface used to control and manage the tests. Measurements are sampled every 0.5 seconds and the mean over 10 samples is recorded (one acquisition every 5 seconds).

Each experimental point was recorded under steady-state conditions. The heat pump was considered to be in steady state when the standard deviation of the main thermodynamic variables remained below the threshold value $\sigma_{tresh} = 0.20$ for at least 5 consecutive minutes of operation (approximately 60 acquisitions), and when variations in ambient temperature and solar irradiance were less than 1°K and 50 W/m², respectively.

The main performance parameters of the heat pump were calculated from the acquired data. The heating capacity supplied by the gas cooler is calculated as shown in Equation (1):

$$\dot{Q}_{GC} = \dot{m}_{ref}\left(h_{in,GG} - h_{out,GC}\right) \tag{1}$$

where the inlet and outlet specific enthalpies are determined using NIST Reference Fluid Thermodynamic and Transport Properties Database (REFPROP), with temperature and pressure measurements on the refrigerant side of the gas cooler as input parameters.

From the measurements obtained with the wattmeter, the total electrical power absorbed by the heat pump can be determined, enabling the calculation of its Coefficient of Performance (COP) using Equation (2).

$$COP = \frac{\dot{Q}_{GC}}{W_{ass,HP}} \tag{2}$$

The uncertainty analysis of the experimental campaign was carried out by evaluating the combined uncertainty (u_C) of the directly measured thermodynamic variables, accounting for both the bias error (u_A) and the instrumental uncertainty (u_B). For indirectly calculated variables, Moffat's error propagation method [16] was applied obtaining 2.87% for COP and 1.42% for $\dot{Q}_{GC}$ with a coverage interval of 95%.

3.2. Main experimental results

Some results of the experimental campaign are reported in Figure 3 and Figure 4 and contribute to provide a comprehensive characterization of the heat pump performance in both operating configurations. This analysis mainly focuses on the dependence of the COP and $\dot{Q}_{GC}$ on the key operating variables: ambient temperature, compressor frequency, and, exclusively for the Sun-Mode, solar irradiance.

In Air-Mode, the performance trends are consistent with the expected thermodynamic behaviour of air-source heat pumps. Both COP and $\dot{Q}_{GC}$ exhibit an almost linear increase with rising ambient temperature. This trend is related to the higher refrigerant evaporation temperature achieved as the ambient temperature increases, which in turn reduces the compression ratio and therefore the power input to the compressor. For example, considering Figure 3 at a fixed compressor frequency of 55 Hz, the COP increases by approximately 11.8% over the tested temperature range, while $\dot{Q}_{GC}$ rises from about 9.8 kW to 11 kW (Figure 4).

The influence of compressor frequency shows a differentiated effect: on one hand, $\dot{Q}_{GC}$ increases significantly due to the higher refrigerant mass flow rate; for instance, from approximately 9.5 kW at 50 Hz to 11.3 kW at 60 Hz at ambient temperature of about 20°C, corresponding to a 19% increase. On the other hand, the impact on efficiency is more limited, as the COP tends to slightly decrease with frequency.

In Sun-Mode, solar irradiance becomes a key variable affecting both efficiency and heating capacity. Under medium-to-high irradiance conditions, the PV/T surface temperature rises substantially, enabling the use of a higher-temperature source than ambient air for refrigerant evaporation. In these favourable conditions, the main heat transfer mechanism is the thermal conduction between the PV module and the sheet-and-tube heat exchanger, leading to improved performance compared to the Air-Mode. For instance, at $f_{comp} = 55\ Hz$ and

$T_{amb} \approx 21°C$, a solar irradiance of approximately 650 W/m² yields a COP in Sun-Mode that is about 4% higher than in Air-Mode.

Conversely, under low irradiance conditions, the PV module temperature drops significantly, reducing the effectiveness of conductive heat transfer. In this regime, natural convection becomes the dominant mechanism, which is thermally less effective than the forced convection provided by the finned-coil evaporator used in Air-Mode. This results in lower evaporation temperatures and a decrease in Sun-Mode performance in these conditions: in fact, at $T_{amb} \approx 21°C$ and irradiance around 350 W/m², the COP decreases from 3.6 in Air-Mode to 3.3 in Sun-Mode.

Also, it is worth noting that Sun-Mode operation generally leads to slightly lower heating capacities compared to Air-Mode at the same compressor frequency as shown in Figure 4. For example, at 60 Hz and 25°C, the heat pump delivers approximately 12 kW in Air-Mode, while the maximum capacity in Sun-Mode is around 11.2 kW. This behaviour can be explained by the higher refrigerant mass flow rate in Air-Mode operation. In fact, at identical compressor frequencies, the mass flow rate in Air-Mode is about 24.1% higher than in Sun-Mode, given similar boundary conditions.

Overall, the experimental data demonstrate that, for each compressor frequency, a critical irradiance threshold that determines whether Sun-Mode operation becomes more advantageous than Air-Mode exists; for this reason, these findings confirm the importance of implementing a predictive control strategy based solely on boundary conditions to maximize prototype performance by dynamically selecting the most efficient heat source.

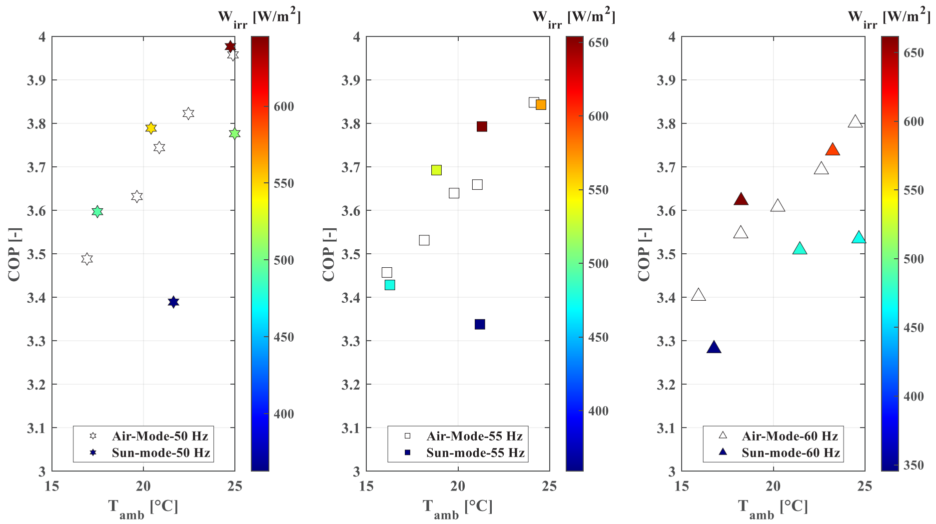

- **Figure 3.** Experimental COP trends in Air-Mode and Sun-Mode for each compressor frequency.

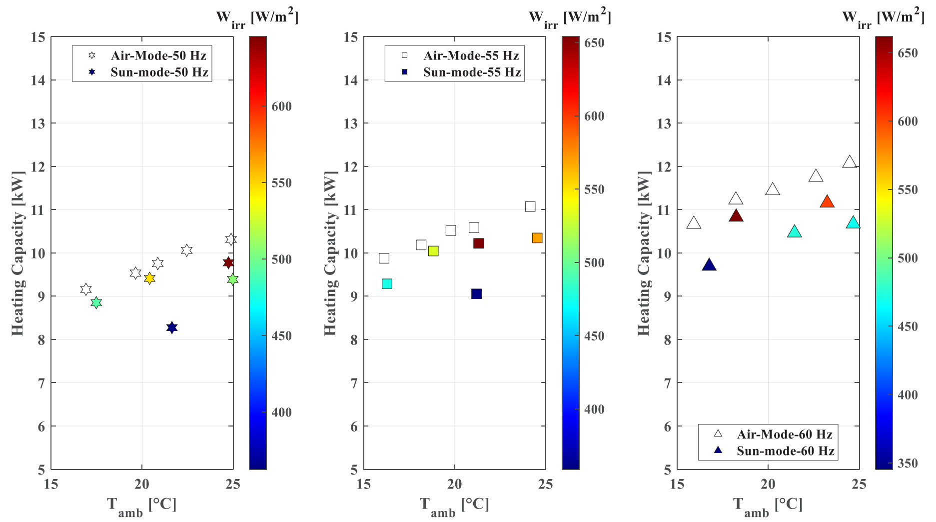

- **Figure 4.** Experimental $\dot{Q}_{GC}$ trends in Air-Mode and Sun-Mode for each compressor frequency.

4. Machine Learning Model

4.1. Model structure and training procedure

The experimental dataset collected during the test campaign was used to train two separate neural networks, one for Air-Mode operation and one for Sun-Mode operation. The objective of developing a Machine Learning model based exclusively on boundary conditions is to enable future implementation of a real-time predictive control strategy capable of managing the switching between the two evaporation sources selecting the one ensuring the highest efficiency.

For this reason, the input variables chosen for training include only the ambient temperature and compressor frequency for Air-Mode, with the addition of solar irradiance for Sun-Mode. The primary output of interest is the COP, although both neural networks were also trained to predict the gas cooler heating capacity.

To guarantee consistent training while preserving representativeness of real-field operation, the dataset was stratified by compressor frequency and then binned across the full operating range of ambient temperature (and solar irradiance for Sun-Mode). Representative samples from each bin were selected for the calibration dataset, ensuring uniform coverage of the operating domain. All remaining points were instead used for model validation. Table 4 reports, for each compressor frequency, the number of calibration and validation points together with the corresponding ranges of ambient temperature (and solar irradiance for Sun-Mode).

Both ANNs were implemented as feed-forward neural networks and the Levenberg-Marquardt algorithm was adopted for training due to its efficiency and robustness on small-to-medium-sized datasets. A standard one-layer architecture with two neurons was chosen to balance predictive accuracy and computational simplicity, making the models suitable for potential real-time control applications.

Table 4. Summary for the calibration and validation dataset of the ML model.

	$Air - Mode$			$Sun - Mode$			
$f_{comp}[Hz]$	T_{amb} range [°C]	N° of points for calibration	N° of points for validation	T_{amb} range [°C]	G range $[W/m^2]$	N° of points for calibration	N° of points for validation
50	16.9 ÷24.8	14	8	17.4÷24.9	275÷725	16	6
55	16.1÷24.1	15	6	16.3÷24.5	226÷727	18	7
60	15.9÷24.7	12	3	16.7÷24.6	264÷692	17	4

4.2. Model Validation

Model validation was performed by comparing the neural network predictions with the experimental measurements in the validation dataset. Two statistical indicators were computed: the Mean Absolute Percentage Error (MAPE) and the Mean Relative Percentage Error (MRPE). In addition, the percentage of validation points falling within a $\pm 5\%$ deviation band $(\delta_{\pm 5\%})$ from the experimental COP measurements was evaluated. The overall validation results for both Air-Mode and Sun-Mode are illustrated in Figure 5 and Figure 6.

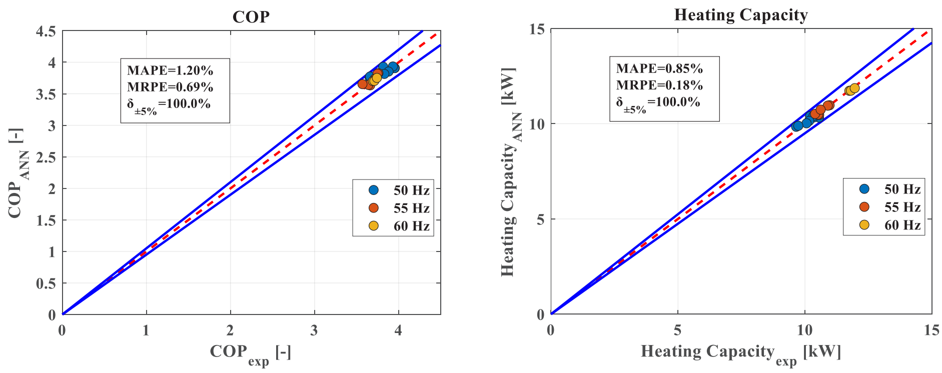

Figure 5. Validation of the Air-Mode ANN.

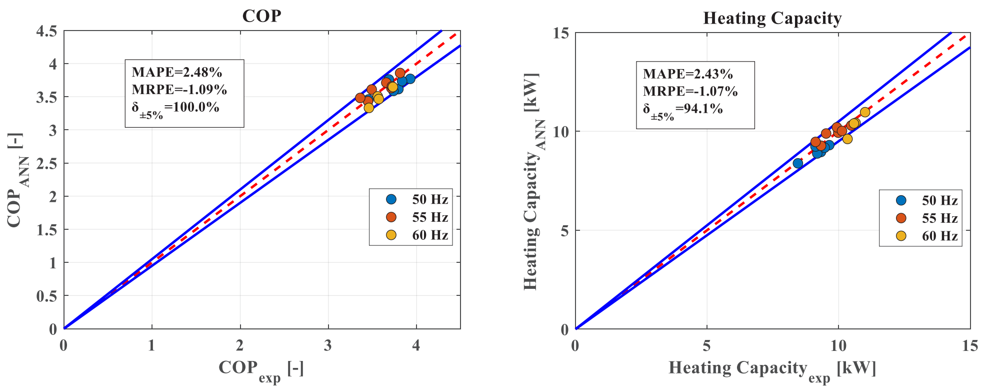

Figure 6. Validation of the Sun-Mode ANN.

5. Results and Discussion

The data generated by the ML models were used to evaluate the combined effect of compressor frequency, ambient temperature, and solar irradiance on the performance of the prototype, and to perform a systematic comparison between the two operating modes.

The performance maps generated with the models and reported in Figure 7 confirm the trends observed in the experimental analysis. For each compressor frequency and each operating mode, COP curves were reconstructed as a function of ambient temperature and of irradiance too, in the case of Sun-Mode, within the range of operating conditions covered by the calibration dataset.

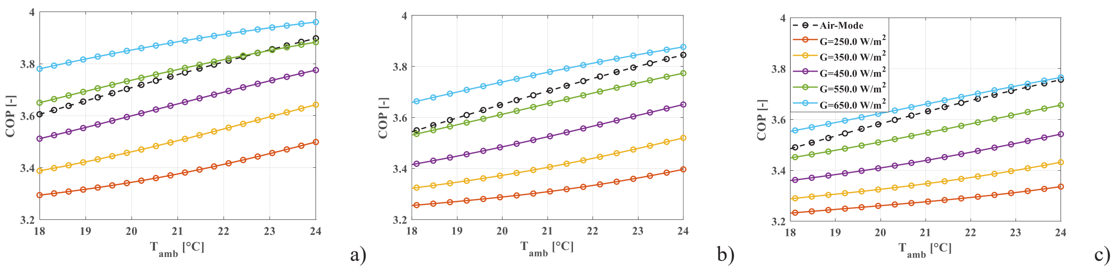

Figure 7. Performance comparison by source at a) 50Hz, b) 55Hz and c) 60Hz.

By interpolating the resulting maps, it was possible to determine, for every value of T_{amb} and for each frequency, a threshold irradiance value G_{thresh} such that the following condition would be satisfied:

$$COP_{SUN-MODE} > COP_{AIR-MODE} \tag{3}$$

This threshold defines the region of the (T_{amb}, G) plane where the solar source becomes more advantageous than the air source, as illustrated in Figure 8.

Consistently with the experimental findings, as the ambient temperature increases, outdoor air becomes an increasingly favourable heat source; therefore, a higher irradiance level is required for Sun-Mode to outperform Air-Mode.

Another trend highlighted by the ML results is the dependence of G_{thresh} on compressor frequency. Overall, as f_{comp} increases, the irradiance required for Sun-Mode to become more efficient tends to rise.

Furthermore, the behaviour of G_{thresh} with respect to T_{amb} appears almost linear and well-defined.

It is important to note that these findings represent a preliminary assessment obtained through the ML model. The reconstruction provided by the algorithm accurately reflects the experimental trends within the calibration domain, but its reliability outside that range should be confirmed expanding the dataset of available experimental points.

Nevertheless, the results show that Sun-Mode becomes particularly attractive at lower ambient temperatures. This could be especially relevant in colder climates, where low ambient temperatures persist for a significant portion of the year. Under these conditions, the irradiance threshold G_{thresh} tends to decrease, making it advantageous to exploit the solar evaporator even when only moderate levels of solar radiation are available. This suggests that, in regions characterized by harsh winter conditions, integrating a PVT evaporator can offer tangible improvements to the overall performance of the heat pump if moderate solar irradiance is available.

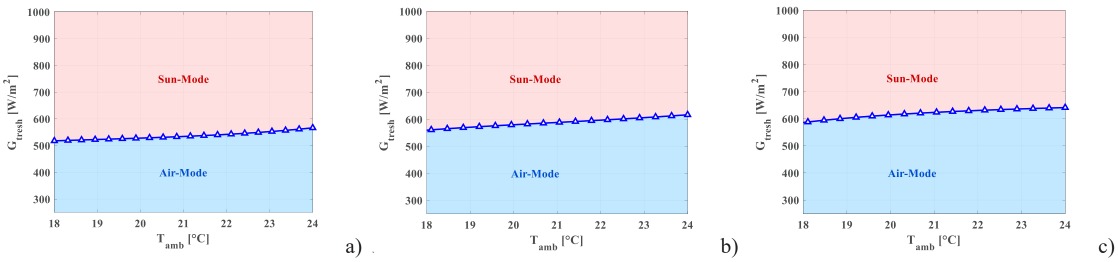

Figure 8. Identification of the irradiance threshold for which the Sun-Mode operation is more convenient than the Air-Mode as a function of the ambient temperature at a) 50Hz, b) 55Hz and c) 60Hz.

6. Conclusions

This work presents the experimental investigation of a dual-source direct-expansion CO_2 heat pump prototype operating in both Air-Mode and Sun-Mode, combined with the development of a ML-based predictive tool aimed at supporting real-time source-switching control strategies. The integration of experimental data and ML modelling enabled a deeper understanding of the system's behavior under a wide range of boundary conditions.

The main findings of this study can be summarized as follows:

- The experimental campaign confirmed the expected thermodynamic behavior of both operating modes, showing that Air-Mode performance improves almost linearly with increasing ambient temperature, whereas Sun-Mode performance strongly depends on solar irradiance and exhibits noticeable advantages under medium-to-high irradiance level.
- For all tested compressor frequencies, the ML models successfully reconstructed the COP trends using only boundary conditions as inputs, accurately replicating the experimental behavior within the calibration domain.
- The ML-generated performance maps enabled the identification of an irradiance threshold (G_{thresh}) for each combination of ambient temperature and compressor frequency, above which Sun-Mode becomes more efficient than Air-Mode. This threshold tends to increase with both ambient temperature and compressor frequency.
- Sun-Mode becomes especially advantageous at lower ambient temperatures, where the irradiance threshold tends to decrease, indicating that, in these conditions, even moderate levels of solar radiation may be sufficient to outperform Air-Mode. This aspect could be particularly promising for cold-climate applications.
- The results confirm the feasibility of implementing a real-time predictive control strategy, capable of selecting the most efficient heat source based exclusively on the boundary conditions (T_{amb}, G) and on compressor frequency, under the specific and constant heat sink conditions considered in the experimental tests.

Overall, the study demonstrates the potential of integrating a PV/T evaporator into a CO_2 heat pump system and highlights the benefits of combining experimental data with machine learning tools to support advanced control strategies. Future work should focus on expanding the training dataset toward lower ambient temperatures, where Sun-Mode appears particularly promising, and on conducting an extended experimental campaign considering lower water temperature levels, typical of space-heating applications. These developments would allow further refinement of the ML models and support the implementation of predictive control strategies in real operating environments.

Acknowledgements

This work was carried out within the Collaboration Agreement ENEA-UNINA, funded by the three-year MASE-ENEA 2022-2024 Research Program for Research on the Italian Electricity System.

Acknowledgement is made to the Ministry of University for funding the DM-118 PA Ph. D scholarship in Industrial Engineering at University of Naples Federico II.

References

[1] Eurostat, 2023, Energy Efficiency - Heating and Cooling.

[2] Eurostat, 2023, Energy Efficiency - Heat Pumps.

[3] European Commission, Directorate-General for Research and Innovation, European Green Deal – Research & innovation call, Publications Office of the European Union, 2021.

[4] International Energy Agency (IEA) - The future of heat pumps, 2023.

[5] European Heat Pump Association (EHPA) - About heat pumps.

[6] Konrad M. E., MacDonald B. D., Cold climate air source heat pumps: Industry progress and thermodynamic analysis of the market-available residential units, *Renewable and Sustainable Energy Reviews* 2023; **118** 113739.

[7] Pelella F.,Zsembinszki G.,Viscito L., Mauro A.W., Cabeza L.F., Thermo-economic optimization of a multi-source (air/sun/ground) residential heat pump with a water/PCM thermal storage, *Applied Energy* 2023; **331** 120398.

[8] Mastrullo R., Mauro A. W., Pelella F., Viscito L., Dual source (air-solar) heat pump: thermo-economic analysis of sizing factors depending on climate conditions, 2022, 15th IIR-Gustav Lorentzen conference on Natural Refrigerants, Trondheim, Norway.

[9] Vallati A., Di Matteo M., Lo Basso G., Ocłon P., Fiorini C. V., Definition of a PVT coupled water source heat pump system through optimization of individual components, *Energy* 2024; **304** 132455.

[10] Besagni L., Croci L., Nesa R., Molinaroli L., Field study of a novel solar-assisted dual-source multifunctional heat, *Applied Energy* 2024; **369** 123478.

[11] Calabrese N., Mastrullo R., Mauro A. W., Rovella P., Tammaro M., Performance analysis of a rooftop, air-to-air heat pump working with CO2, *Applied Thermal Engineering* 2015; **75** 1046-1054.

[12] Boccardi G., Botticella F., Lillo G., Mastrullo R., Mauro A. W., Trinchieri R., Experimental investigation on the performance of a transcritical CO2 heat pump with multi-ejector expansion system, *International Journal of Refrigeration* 2017; **81** 389-400.

[13] Zanetti E., Azzolin M., Girotto S., Del Col D., Performance and control of a CO2 dual source solar assisted heat pump with a photovoltaic-thermal evaporator, *Applied Thermal Engineering* 2023; **218** 119286.

[14] Bhadra S., Mwesigye A.,Influence of control strategy on the energetic performance of an air source heat pump coupled with a solar air collector for domestic hot water in a cold climate, *Renewable Energy* 2025; **244** 122682.

[15] Di Salvatore F., Mauro A. W., Trinchieri R., Viscito L., Experimental characterization of a carbon-dioxide dual source heat pump; *J. Phys.: Conf. Ser.* 2025; **3143 (1)** 012107.

[16] Shaker L. M., Al-Amiery A. A., Hanoon M. M., Kadhum A. A. H., Examining the influence of thermal effects on solar cells: a comprehensive review, *Sustainable Energy Research* 2024; 11:6.

[17] Moffat R. J., Using uncertainty analysis in the panning of an experiment, *Journal of Fluids Engineering* 1985; **107 (2)** 173–178.